AIP | Journal of Applied Physics

First-principles study of atomic hydrogen adsorption and initial hydrogenation of Zr(0001) surface

Peng Zhang, Shuangxi Wang, Jian Zhao, Chaohui He, Yaolin Zhao et al.

Citation: J. Appl. Phys. **113**, 013706 (2013); doi: 10.1063/1.4772675
View online: http://dx.doi.org/10.1063/1.4772675
View Table of Contents: http://jap.aip.org/resource/1/JAPIAU/v113/i1
Published by the AIP Publishing LLC.

JOURNAL OF APPLIED PHYSICS **113**, 013706 (2013)

First-principles study of atomic hydrogen adsorption and initial hydrogenation of Zr(0001) surface

Peng Zhang,[1,a)] Shuangxi Wang,[2] Jian Zhao,[3] Chaohui He,[1] Yaolin Zhao,[1] and Ping Zhang[4,b)]
[1]*Department of Nuclear Science and Technology, Xi'an Jiaotong University, Xi'an 710049, People's Republic of China*
[2]*State Key Laboratory for Superlattices and Microstructures, Institute of Semiconductors, Chinese Academy of Sciences, P. O. Box 912, Beijing 100083, People's Republic of China*
[3]*State Key Laboratory for Geomechanics and Deep Underground Engineering, China University of Mining and Technology, Beijing 100083, People's Republic of China*
[4]*LCP, Institute of Applied Physics and Computational Mathematics, Beijing 100088, People's Republic of China*

(Received 16 October 2012; accepted 4 December 2012; published online 3 January 2013)

The atomic hydrogen adsorption on Zr(0001) surface is systematically investigated by using density functional theory within the generalized gradient approximation and a supercell approach. The coverage dependence of the adsorption structures and energetics is studied in detail for a wide range from 0.11 to 2.0 monolayer. At low coverage of $0 < \Theta \leq 1.0$, the most stable adsorption site is identified as the on-surface hcp site followed by the fcc site, and the adsorption energy gradually increases with the coverage, thus, indicating the higher stability of on-surface adsorption and the tendency to form H clusters. The origin of this stability is carefully analyzed by the projected density of states and the charge distribution showing the Zr-H chemical bonding with a mixed ionic/covalent feature during the surface hydrogenation. In addition, the minimum energy paths as well as the activation barriers of the on-surface diffusion and the penetration from on-surface sites to subsurface sites are also calculated. At high coverage of $1.0 < \Theta \leq 2.0$, it is found that the co-adsorption configuration with 1.0 monolayer H residing on the surface hcp sites and the remaining $(\Theta - 1)$ monolayer H occupying the sub-surface octahedral sites is most energetically favorable. The electronic structure properties of the resultant H-Zr-H sandwich structures at the coverage range of $1.0 < \Theta \leq 2.0$ reveal the similar characteristics to the bulk hydride ZrH_2, providing a detailed microscopic understanding for the Zr surface hydrogenation phenomenon. © *2013 American Institute of Physics*. [http://dx.doi.org/10.1063/1.4772675]

I. INTRODUCTION

A fundamental understanding of the nature of the interaction between hydrogen and transition metal surfaces is crucial to elucidate the role of hydrogen in a series of important technological processes, such as hydrogenation, corrosion, and heterogeneous catalysis.[1] More specifically, hydrogen degradation of the structural properties of solids, referred as hydrogen embrittlement (HE), is an elementary problem in materials physics. The understanding of HE in metals has already turned into a key issue of materials science and engineering.[2] Particularly, it plays an important role in the nuclear industry where the cladding materials of nuclear fuel are made of zirconium and its alloys. These are submitted to the severe storage as well as the service condition, involving with the hydrogen contact and penetration.[3] Therefore, a thorough investigation based on the parameter-free, *ab initio* calculations is required to probe into the microscopic physics responsible for the macroscopic behavior of these materials.

Since the early 1980s, much efforts have been devoted to try to understand the hydrogen behavior in zirconium,[4–11] although most of those were concerned with the practical Zr alloys and bulk reactions. Stojilovic *et al.*[12] reviewed the characteristics of Zr(0001) surface chemistry by summarizing a series of experimental measurements on the hydrogen segregation and diffusion properties. On the other hand, some theoretical works have been recently carried out to investigate the bulk properties of Zr-H system.[13,14] In addition, Yamamoto *et al.*[15] calculated the adsorption potential of hydrogen atom on Zr(0001) surface by an effective medium theory in earlier 1990s. Furthermore, the adsorption and dissociation of H_2 molecules on Zr(0001) surface were systematically studied in our previous work.[16] Through calculating the adiabatic potential energy surface, the chemisorbed molecular adsorption states were identified to be along the parallel channel at the top site. Meanwhile, the most stable and favorable channel for the dissociative adsorption of H_2 was found and the hcp site turned out to be the most stable equilibrium adsorption site for hydrogen atom on Zr(0001) surface after the dissociation. However, to the best of our knowledge, no more theoretical studies, especially from the basic quantum mechanical electronic structure calculations, have been performed to give an insight into the atomic hydrogen adsorption on Zr(0001) surface. It is considered as a very important stage of the incipient hydrogenation of the Zr surface.

Motivated by these observations, in this paper, we present a detailed first-principles study by investigating the

[a)]Electronic mail: pengzhang@xjtu.edu.cn.
[b)]Electronic mail: zhang_ping@iapcm.ac.cn.

dependence of the atomic hydrogen adsorption properties on a variety of coverages ranging from 0.11 to 2.0 monolayers (ML). Through a series of total energy calculations, we analyze and discuss the atomic hydrogen adsorption configurations, the Zr-H chemical bonding characteristics, and the minimum energy paths (MEP) of the surface diffusion and penetration of atomic hydrogen on Zr(0001) surface. In the analysis of the adsorption energies and behaviors at different coverages, we obtain the saturation coverage of 1.0 ML on surface and show the favorable H-Zr-H sandwich structure at the coverage larger than 1.0 ML. Particularly, it gives a microscopic picture on the atomic hydrogen adsorption at high coverage and the transition to the metal hydride. In summary, our present *ab initio* study further provides a valuable insight into the incipient hydrogenation of Zr(0001) surface.

II. METHOD

The first-principles total energy calculations based on the density functional theory (DFT) are self-consistently carried out using the Vienna *ab initio* simulation package (VASP).[17] The generalized gradient approximation (GGA) introduced by Perdew, Burke, and Ernzerhof (PBE)[18] and the projector-augmented wave (PAW) pseudopotentials[19] are employed to describe the electron exchange-correlation energy and the electron-ion interaction, respectively. The cutoff energy for the plane-wave expansion is set to 350 eV. The clean Zr(0001) surface is modeled by a repeated slab which is composed of five atomic layers separated by a vacuum region of 20 Å, which is tested to be sufficiently convergent. The hydrogen atoms are only adsorbed on one side of the slab, where the induced dipole moment is taken into account by applying a dipole correction.[20] In our calculations, the three topmost Zr layers as well as the adsorbed H atoms are fully relaxed until the forces on the atoms are less than 0.02 eV/Å. Test calculation shows that the spin of this adsorbate-substrate system is negligible. Therefore, non-spin-polarization calculations are adopted throughout the present work. We have used $(13 \times 13 \times 1)$ k-point grid for the $p(1 \times 1)$ surface cell, $(7 \times 7 \times 1)$ k-point grid for the $p(\sqrt{3} \times \sqrt{3})$ and $p(2 \times 2)$ cells, and $(5 \times 5 \times 1)$ k-point grid for the $p(3 \times 3)$ cell, according to the Monkhorst-Pack scheme[21] to integrate over the Brillouin zone of the Zr(0001) surface. In addition, a temperature broadening parameter of 0.1 eV is chosen to smear the occupation of the bands around the Fermi energy by a finite-T Fermi function[22] and extrapolating to $T = 0$ K.

In this work, the total energy calculations for the hydrogen atoms at the seven high symmetry adsorption sites including both on-surface (top, bri, hcp, and fcc) and subsurface (tetrahedral-I, tetrahedral-II, and octahedral) sites schematically depicted in Fig. 1 have been implemented for the coverage ranging from 0.11 to 2.00 ML. The tetrahedral-I site is the tetrahedra site I which has four nearest neighbor Zr atoms, three atoms above and one right below with respect to the normal direction of the Zr(0001) surface. And the tetrahedral-II site is the tetrahedral site II similar to the tetrahedral-I site, which correspondingly has one atom right above and three below. Moreover, the octahedral site is the site which has six nearest neighbor Zr atoms (three above and three below).

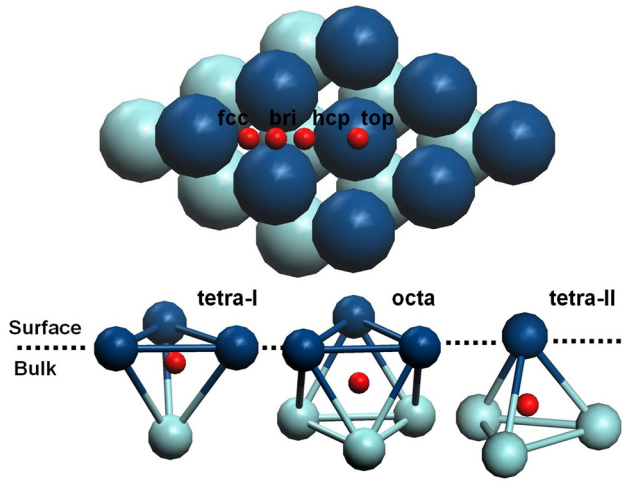

FIG. 1. The hydrogen adsorption sites on the Zr(0001) surface. The upper panel is the top view of Zr(0001) surface including the on-surface fcc, bri, hcp, and top adsorption sites, respectively. The lower three plots are the side views for the subsurface adsorption sites including the tetrahedral-I, octahedral, and tetrahedral-II sites. Cyan and blue balls represent for the topmost and the second Zr layer, respectively, and red balls represent for H atoms.

More specifically, the hydrogen coverage of 0.11 and 0.33 ML is calculated using the $p(3 \times 3)$ surface unit cell, while the coverage of 0.25, 0.50, 0.75, 1.00, 1.25, 1.5, 1.75, and 2.00 ML is calculated in the $p(2 \times 2)$ surface cell. After the geometry optimization calculations of the atomic adsorption at those considered sites, it is found that the hydrogen adsorptions at the on-surface top and bri sites are unstable by the observation that after the relaxation, the hydrogen atom initially located at the bri site will move to the fcc site for instance. Additionally, the sub-surface tetrahedral-I site at low coverage is also found to be unstable due to the fact that the hydrogen atom placed on this subsurface site will penetrate upward to a surface site after the relaxation. As a result, in the present paper, the on-surface adsorption investigations are only focused on the hcp and fcc sites, and the tetrahedral-II and octahedral sites are considered for the subsurface adsorption.

The central quantity tailored for this work is the average adsorption energy per hydrogen atom with respect to the hydrogen molecule in gas phase, defined as

$$E_{ad} = -\frac{1}{N_H}\left[E_{H/Zr(0001)} - E_{Zr(0001)} - N_H\frac{1}{2}E_{H_2}\right], \quad (1)$$

where N_H is the total number of H atoms presented in the adsorption system, $E_{H/Zr(0001)}$, $E_{Zr(0001)}$, and E_{H_2} are the total energies of the optimized slab containing hydrogen atoms, the corresponding clean Zr(0001) slab, and a free H_2 molecule, respectively. According to this definition, a positive value of E_{ad} indicates that the adsorption is exothermic (stable) with respect to a free H_2 molecule while the negative is endothermic (unstable).

III. RESULTS AND DISCUSSIONS

A. Bulk Zr, clean Zr(0001) surface, hydrogen molecule

Before studying the H adsorption on the Zr(0001) surface, we first consider the bulk hcp Zr and the clean

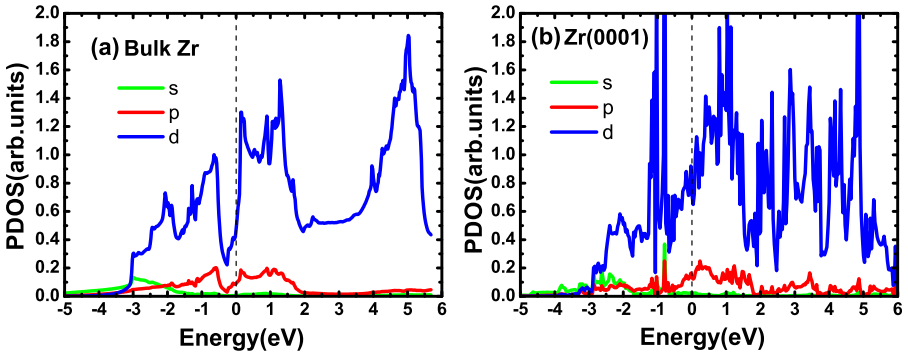

FIG. 2. (a) The PDOS of bulk hcp Zr and (b) the PDOS for the topmost layer of clean $p(2\times2)-\mathrm{Zr}(0001)$ surface. The Fermi energy is set at zero.

Zr(0001) surface. The present optimized equilibrium lattice parameters and bulk modulus obtained by fitting the energy-volume data in the third-order Birch-Murnaghan equation of states (EOS)[23] are $a=3.24$ Å, $c/a=1.60$, and $B=93.6$ GPa, well comparable to the experimental measurements of 3.23 Å, 1.59, and 92 GPa.[24] The calculated cohesive energy of the bulk hcp Zr is 6.14 eV, also in good agreement with the experimental value of 6.25 eV.[25] The orbital-resolved partial density of states (PDOS) per atom for bulk Zr is shown in Fig. 2(a) with the Fermi level set at zero. The *d* occupation of the energy band is substantially broad and the bottom of the band is of *s* character with a local minimum near the Fermi level.

The calculations for the geometry relaxation of the clean Zr(0001) surface with 1×1, $\sqrt{3}\times\sqrt{3}$, 2×2, and 3×3 periodicities not only provide a test on the clean surface with different cell sizes, but are also used to evaluate the charge density difference discussed later and assess the change in the work function through the hydrogen adsorption at different coverages. As for the clean $p(2\times2)$-Zr(0001) surface, we perform a geometry optimization and calculate the interlayer relaxations $\Delta_{ij}=(d_{ij}-d_0)/d_0$ with respect to the bulk interlayer distance $d_0=2.590$ Å. The first-second interlayer contraction is about 6.8% while the second-third interlayer expansion is nearly 2.5%. Moreover, the calculated surface energy $E_s=0.92\,\mathrm{eV/atom}$ and the work function $\Phi=4.23$ eV are both consistent well with pervious theoretical and experimental results.[25,26] As one knows, the calculation of surface properties requires a sufficiently dense *k*-point mesh, efficient energy cutoff, the correct model, and other details to minimize the numerical errors. To test the convergency of the physical properties of the clean Zr(0001) surface, we have carefully calculated the surface energy E_s and the work function Φ of the Zr(0001) slabs by using different models with various *k*-point meshes. As listed in Table I, these results reveal that the influence on the surface energetics from different models is negligibly small. Fig. 2(b) gives the PDOS of the topmost layer of the clean Zr(0001) surface, showing that the *d* occupation around the Fermi energy is increased at the top layer of clean Zr(0001) compared with the bulk Zr. This implies that there are surface states and resonances near the Fermi level and the *d* electrons are responsible for the marked adsorption properties. We do not consider the quantum size effects on the atomic and electronic structures, since in our various supercell models the substrate has been fixed with the same thickness.

On the other hand, the total energies of the isolated H atom and free H_2 molecule are both calculated in an orthorhombic cell of $15\times16\times17$ Å^3 with a $(3\times3\times3)$ *k*-point mesh for sampling. The binding energy of H_2 is determined to be 4.52 eV, the H-H bond length $d=0.75$ Å, and the vibrational frequency $\omega=4287\,\mathrm{cm^{-1}}$, corresponding to a zero-point energy (ZPE) of 0.266 eV, which are all well comparable with the experimental results and the theoretical predictions.[27] In the present work, the ZPE is neglected due to the slightly relative difference among various absorption configurations. Therefore, all the calculated results above affirm that the present work can provide a reliable description for H-Zr system.

B. Atomic hydrogen adsorption at $\Theta \le 1.0$

At first, we mainly concentrate on the hydrogen adsorption in the coverage regime of $0<\Theta\le1.0$. The above-mentioned fact that the on-surface top and bri sites, as well as the subsurface tetrahedral-I site, are unstable for the hydrogen adsorption, our systematic calculations have been performed for the remaining four high symmetry adsorption sites, i.e., the on-surface hcp and fcc sites together with the subsurface tetrahedral-II and octahedral sites. The calculated adsorption energies of hydrogen atoms at the four on-surface and subsurface sites with their corresponding work function results are summarized in Table II for different hydrogen coverages in the regime of $0<\Theta\le1.0$. It is clearly seen that all the considered adsorption configurations are stable and the adsorption energies for the on-surface adsorption are always larger than those for the subsurface adsorption, revealing that the hydrogen on-surface adsorption is more energetically favorable than the subsurface adsorption. It is

TABLE I. The calculated results of the surface energy E_s (eV) and the work function Φ (eV) for the clean Zr(0001) surfaces in different *k*-point meshes.

Model	*k*-point mesh	E_s (eV)	Φ (eV)
1×1	$13\times13\times1$	0.9282	4.229
1×1	$15\times15\times1$	0.9372	4.238
2×2	$7\times7\times1$	0.9203	4.231
2×2	$9\times9\times1$	0.9227	4.236
$\sqrt{3}\times\sqrt{3}$	$7\times7\times1$	0.9200	4.215
$\sqrt{3}\times\sqrt{3}$	$9\times9\times1$	0.9265	4.223
3×3	$5\times5\times1$	0.9213	4.224
3×3	$7\times7\times1$	0.9232	4.229

TABLE II. The calculated atomic adsorption energy E_{ad} (eV/atom) and work function Φ (eV) as the function of the atomic hydrogen coverage at different sites of Zr(0001) surface.

Property	Site	$\Theta = 0.11$	$\Theta = 0.25$	$\Theta = 0.33$	$\Theta = 0.50$	$\Theta = 0.75$	$\Theta = 1.00$
E_{ad}	hcp	1.022	1.030	1.051	1.055	1.069	1.077
	fcc	0.958	0.976	0.980	0.996	1.013	1.030
	octa	0.362	0.356	0.343	0.340	0.340	0.352
	tetra-II	0.213	0.371	0.422	0.439	0.463	0.498
Φ	hcp	4.215	4.193	4.208	4.181	4.205	4.290
	fcc	4.213	4.196	4.189	4.171	4.153	4.144
	octa	4.231	4.233	4.243	4.276	4.307	4.315
	tetra-II	4.203	4.189	4.170	4.169	4.139	4.116

indicated that in the coverage range of $0 < \Theta \leq 1.0$, the added hydrogen atom will not spontaneously penetrate into the subsurface in the case of pure on-surface adsorption. Moreover, we can conclude that the hcp site is more stable than the fcc site for the on-surface adsorption, meanwhile the octahedral site is always less stable than the tetrahedral-II site for the subsurface adsorption, consistent well with the experimental and theoretical fact[13,15] that the hydrogen atoms prefer to occupy the tetragonal sites in bulk Zr. For the on-surface adsorption, the adsorption energy increases with the hydrogen coverage showing a prominent attraction between the adsorbate and the substrate and a tendency to form the H islands or clusters on the Zr(0001) surface at $0 < \Theta \leq 1.0$. To further clarify our observation that the hydrogen adsorbates tend to cluster on the Zr(0001) surface, here we take two typical arrangements for the hydrogen adsorbates on the hcp site at the same coverage $\Theta = 0.33$. These two adsorbate configurations are given in Fig. 3. Fig. 3(a) corresponds to the case of a $p(\sqrt{3} \times \sqrt{3})$ surface cell, and Fig. 3(b) gives one selective adsorbate arrangement generated from the $p(3 \times 3)$ surface cell. It is seen that the hydrogen adatoms in Fig. 3(b) are more clustered than those in Fig. 3(a). After the geometry optimization, the calculated adsorption energy is $E_{ad} = 1.021$ eV for the Fig. 3(a) and $E_{ad} = 1.051$ eV for the Fig. 3(b), which shows the preference for the formation of hydrogen clusters on the Zr(0001) surface, in fair accordance with the results listed in Table II. On the other hand, from Table II, we can see that the work function steadily decreases with the hydrogen coverage for both on-surface and subsurface adsorption except for the case at

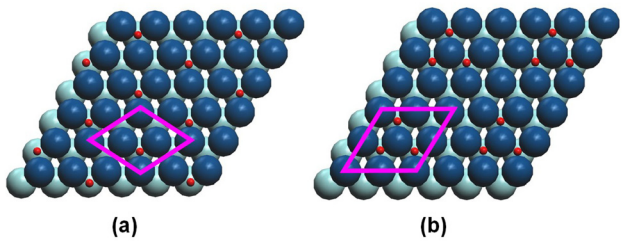

FIG. 3. Two kinds of atomic hydrogen adsorption configurations at the hcp site of Zr(0001) surface at the same coverage $\Theta = 0.33$. The hydrogen adatoms in (b) are arranged to be clustered in the $p(3 \times 3)$-Zr(0001) surface cell, while (a) gives a uniform distribution of the $p(\sqrt{3} \times \sqrt{3})$-Zr(0001) surface model.

TABLE III. The calculated adsorbate height h_{H-Zr} (Å), the bond length R_{H-Zr} (Å), and the topmost interlayer relaxation Δ_{12} (%) for different coverages of atomic hydrogen adsorption at the hcp and fcc sites on Zr(0001) surface.

	h_{H-Zr}		R_{H-Zr}		Δ_{12}	
Θ	hcp	fcc	hcp	fcc	hcp	fcc
0.11	1.102	1.053	2.124	2.150	−3.527	−6.707
0.25	1.089	1.084	2.131	2.160	−4.317	−5.886
0.33	1.099	1.095	2.132	2.165	−3.256	−8.005
0.50	1.067	1.093	2.132	2.157	−2.571	−6.573
0.75	1.066	1.078	2.141	2.157	−2.183	−3.924
1.00	1.048	1.075	2.143	2.157	−2.385	−3.597

the octahedral site. For the on-surface adsorption, one can see that the work function for the fcc adsorption is always lower than that for the hcp adsorption, indicating that the surface charge polarization effect is more prominent for the fcc adsorption than for the hcp adsorption in our considered coverage. As for the subsurface adsorption, the octahedral-adsorbed work function is always higher than that for the tetrahedral-II adsorption.

Our calculated results of the equilibrium geometry properties after the relaxations are presented in Table III, including the height h_{H-Zr} of H above the Zr(0001) surface, the H-Zr bond length R_{H-Zr}, and the topmost interlayer relaxation Δ_{12} for various coverages with hydrogen at the hcp and fcc sites. The atomic hydrogen is located at the initial height of 1.0 Å and the equilibrium adsorption state of the atomic hydrogen at the hcp and fcc sites are both slightly higher than 1.0 Å. Specifically, the height of H above the Zr(0001) surface at the hcp site is relatively higher than that at the fcc site at the low coverage. Concerning the H-Zr bond length R_{H-Zr} at different coverages, it is clearly seen from Table III that for both hcp and fcc adsorptions, the H-Zr bond length varies a little around 2.1 Å as the coverage Θ increases. The shorter bond length at the hcp site implies a stronger interaction between the hydrogen adsorbate and the Zr substrate, which is in good accordance with the obtained result that the hcp site is more stable than the fcc site for on-surface adsorption. The induced topmost interlayer relaxation shows the common contraction for the coverage regime of $0 < \Theta \leq 1.0$, and the notable change is relatively less for the hcp adsorption at a series of the hydrogen coverages.

Now we turn to analyze the electronic properties of the H/Zr(0001) system considering the orbital-resolved PDOS for the H-covered at the hcp site of Zr(0001) surface from the coverage 0.11 ML to 1.00 ML, illustrated in Fig. 4. The Zr *4d* electronic states prominently prevail at the whole energy range from −3.0 eV to 2.0 eV. There appears some new peaks for the electronic states of Zr(0001) surface below the energy −4.0 eV, aligning in the energy with the orbital occupations of the absorbed hydrogen atoms. As it shown, the density of states in the region between −6 and −4 eV indicates the formation of the bonding and antibonding states between the H *1s* and Zr *4d* atomic orbital. Consequently, as the hydrogen coverage increases, some minor changes of the

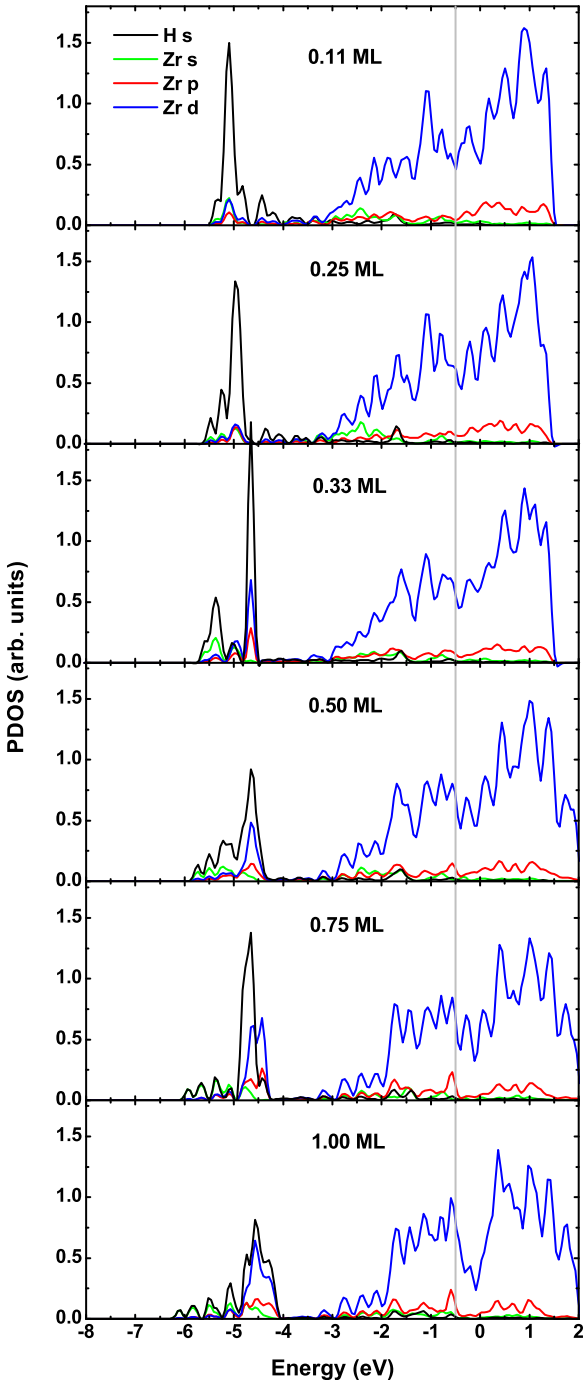

FIG. 4. The PDOS for the on-surface adsorbed hydrogen at the hcp site and the topmost Zr atom at the coverage of 0.11, 0.25, 0.33, 0.50, 0.75, and 1.00 ML, respectively. The Fermi energy is set at zero.

PDOS shape in the energy range of −6 and −4 eV are mainly attributed to the increasing hybridization of H *1s* orbital with Zr *4d* band. The hybridization becomes stronger as the function of coverage, explicitly rationalizing the enhanced interaction between the adsorbate H and the substrate Zr surface. This conclusion is also in good accordance with the calculated adsorption energies as a function of the coverage given in Table III. Further, to gain more insights into the nature of the Zr-H bonding during the atomic hydrogen adsorption onto the Zr(0001) surface, we analyze the difference electron density $\Delta\rho(\mathbf{r})$ for the stable adsorption

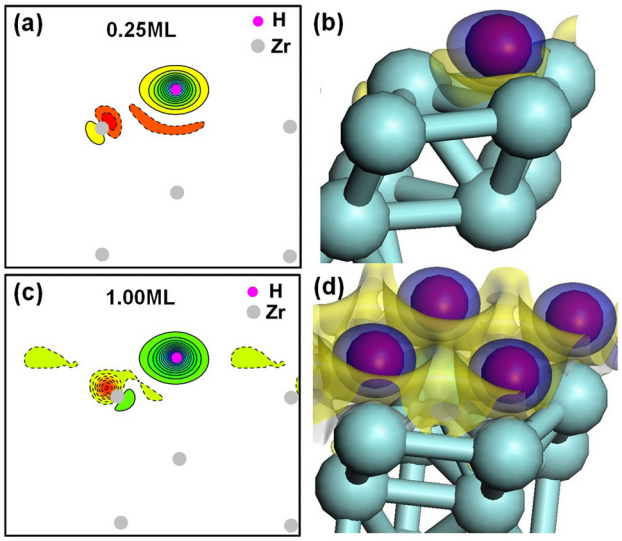

FIG. 5. Difference electron density for the stable atomic hydrogen adsorption state at the hcp site of the Zr(0001) surface. (a) and (c) are 2D figures separately with the coverage $\Theta = 0.25$ and $\Theta = 1.00$ ML. Magenta and gray balls denote H and Zr atoms, respectively. Solid and dashed lines represent charge accumulation and depletion, respectively. (b) and (d) are 3D figures separately with the coverage $\Theta = 0.25$ and $\Theta = 1.00$ ML. Red and cyan balls denote H and Zr atoms, respectively. The shallow blue and yellow colors represent charge accumulation and depletion, respectively.

states at the hcp site of Zr(0001) surface at the coverage 0.25 ML and 1.00 ML, respectively. Here $\Delta\rho(\mathbf{r})$ is obtained by subtracting the electron densities of noninteracting component systems, $\rho^{Zr(0001)}(\mathbf{r}) + \rho^{H}(\mathbf{r})$, from the density $\rho(\mathbf{r})$ of the H/Zr(0001) system, while retaining the atomic positions of the component systems at the same location as in H/Zr(0001) system. The calculated $\Delta\rho(\mathbf{r})$ for the adsorption states are shown in Fig. 5. It is clearly seen that the charge redistribution mainly occurs at the surface and involves the H adatom and the topmost Zr(0001) layer. Specifically, the electrons flow apparently from the Zr *4d* state into H *1s* state, resulting in a depletion of the surface metallic electrons. As the hydrogen coverage increases, the more Zr *4d* electrons transfer to the localized H *1s* orbital. On the other hand, the charge accumulation around the H adatom also occurs along the Zr-H bond, revealing an existence of the covalency. As a result, one can see that the chemical bonding between the H adatom and the surface Zr atom is a characteristic mixture of the ionic and covalent bonding. For pure ZrH_2 with face-centered tetragonal structure, our theoretical studies[28] have shown that the bulk Zr-H chemical bonding also has a mixed ionic/covalent nature. As shown in Fig. 5, like other hydrogen/metal systems, the influence of the adsorbed Zr(0001) surface is rapidly screened out as going into the bulk. Besides, the bonding character of the inner Zr layers is essentially identical to the bulk case, reflecting that there are negligibly small changes in the interior of the Zr slab at both low ($\Theta = 0.25$) and high ($\Theta = 1.00$) coverages.

After elucidating the chemical bonding properties for the most stable adsorption configuration, we particularly concentrate on the migration characteristics of the H adatom when it undergoes the in-plane diffusion and the interplane penetration separately. The atomic hydrogen diffusion after the on-surface dissociation of H_2 is an elementary process of

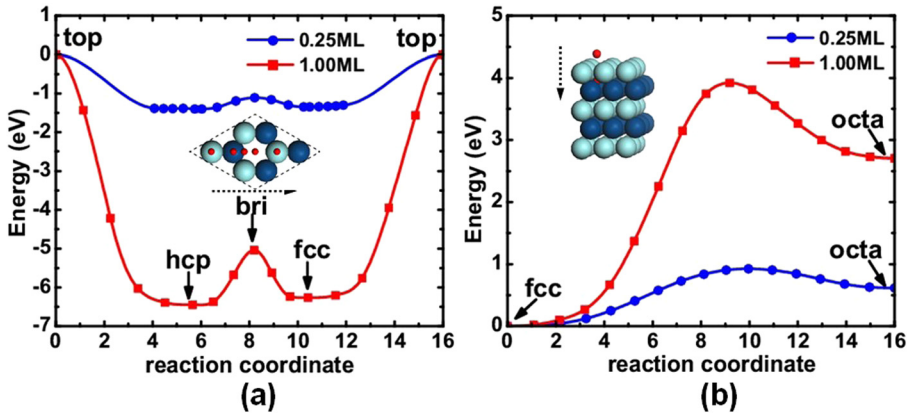

FIG. 6. MEP of (a) the on-surface diffusion and (b) the penetration from on-surface fcc to sub-surface octahedral site for the H adatom on the Zr(0001) surface with the coverage $\Theta = 0.25$ and $\Theta = 1.00$ ML, respectively. The insets schematically show the atomic geometries along the diffusion and penetration paths.

the surface hydrogenation and plays an important role in understanding many catalytic reactions. Besides, the hydrogen penetration into the subsurface and bulk region is also critical for the transition and formation of the zirconium hydride. Therefore, the climbing image-nudged elastic band (CINEB) method[29] is adopted to determine the energy barriers and the MEP for the initial stage of the hydrogenation, corresponding to both the on-surface diffusion and the penetration from surface to subsurface. The CINEB is an efficient and improved method for finding the energy saddle point between the given initial and final states to understand the MEP of the detailed diffusion behavior. The transition path is represented computationally by a sequence of 17 configurations (images) between the initial and final states and a linear interpolation in all atomic coordinates is used as an initial guess. The calculated MEPs of surface diffusion and penetration at both $\Theta = 0.25$ and $\Theta = 1.00$ are shown in Fig. 6. From Fig. 6(a), it is also indicated the relative stability of the H adsorption among various on-surface sites, i.e., the fcc site is less stable than the hcp site within the coverage of $0 < \Theta \leq 1.0$. Our calculated diffusion barriers from hcp to fcc site on the surface are 0.29 eV at $\Theta = 0.25$ and 1.40 eV at $\Theta = 1.00$, respectively, implying that the diffusion becomes much difficult at higher coverage. As the coverage gets close to $\Theta = 1.00$, the hcp sites of H/Zr(0001) surface are mainly occupied first and will be able to form hydrogen clusters at low temperature. On the other hand, the energetics of the H adatom along the penetration path also shows sensitive dependence on the coverage. Since there is no geometric obstacle between the neighboring fcc and octahedral sites, it is natural to speculate a possible penetration from the fcc site on surface to the nearest octahedral site beneath in the subsurface. The calculated MEP of this penetration at both $\Theta = 0.25$ and $\Theta = 1.00$ is presented in Fig. 6(b). It is carefully found in both cases that the saddle points correspond to the same geometry that the hydrogen atom is just in the plane of the topmost Zr layer. Moreover, the calculated energy barrier of the penetration from the fcc to octahedral site is as large as 0.93 eV at the low coverage of $\Theta = 0.25$. As the coverage increases to $\Theta = 1.00$, unexpectedly, the barrier which the four hydrogen atoms need to overcome to simultaneously penetrate into the sub-surface octahedral site largely advances to 3.92 eV. The sharp raise in energy barrier given in Fig. 6(b) suggests that the probability of the low temperature interlayer penetration of H on Zr(0001) surface is negligibly small in the coverage range of $0 < \Theta \leq 1.0$. In addition, we take another consideration that only one hydrogen atom penetrates into the sub-surface from the fcc site to the octahedral site at the same coverage $\Theta = 1.00$ and the obtained migration barrier decreases to 0.92 eV. It turns out to be a trivial normalization effect. The migration barrier per H atom stays more or less the same or even is slightly decreased at the coverage of 1.00 ML. From this point, we can see that the H atoms may still be absorbed in the sub-surface region at the high coverage with pre-adsorbed hydrogen atoms on the surface. To clarify the stability of the co-adsorption configurations in the coverage range of $0 < \Theta \leq 1.0$, we systematically investigate the structures that there are 0.25 ML H atoms in the three particular subsurface sites (octahedral, tetrahedral-I, and tetrahedral-II) and additional 0.25 ML, 0.50 ML, 0.75 ML H atoms at the on-surface hcp and fcc sites, respectively. The calculated adsorption energy of each configuration is listed in Table IV. It is clearly seen that the hcp site is still energetically favorable for the co-adsorption at the octahedral and tetrahedral-II sites. Moreover, at the same total coverage, the obtained adsorption energies for co-adsorption structures are a little lower compared to the configuration where the H atoms are purely adsorbed on the surface hcp sites or fcc sites correspondingly. For instance, the calculated adsorption energies are 0.811, 0.734, and 0.827 eV, respectively, at the hcp site for the total coverage $\Theta = 0.75$, in comparison with the 1.069 eV from Table II when all the H atoms are adsorbed at the surface hcp sites. These calculations above reveal that for hydrogen adsorption coverage up to 1 ML, the hydrogen atoms prefer energetically to stay on the surface.

TABLE IV. The calculated adsorption energy E_{ad} (eV/atom) for the structures with mixed subsurface (octahedral, tetrahedral-I, and tetrahedral-II) and on-surface (hcp and fcc) hydrogens. The total coverage is indicated at the bottom.

$\Theta_{sub} = 0.25$	$\Theta_{on} = 0.25$		$\Theta_{on} = 0.50$		$\Theta_{on} = 0.75$	
Sites	Hcp	Fcc	Hcp	Fcc	Hcp	Fcc
Octa	0.697	0.644	0.811	0.780	0.936	0.858
Tetra-I	0.551	0.646	0.734	0.764	0.836	0.834
Tetra-II	0.742	0.692	0.827	0.792	0.908	0.868
Θ_{total}	0.50		0.75		1.00	

TABLE V. The calculated atomic adsorption energy E_{ad} (eV/atom), the first interlayer relaxation Δ_{12} (%), and the bond length R_{H-Zr} (Å) for the atomic hydrogen adsorption on Zr(0001) surface in the coverage of $1.0 < \Theta \leq 2.0$.

Property	$\Theta = 1.25$	$\Theta = 1.50$	$\Theta = 1.75$	$\Theta = 2.00$
E_{ad}	0.951	0.858	0.771	0.698
Δ_{12}	−5.333	−1.573	−0.551	+2.833
R_{H-Zr}	2.014	2.006	1.994	1.961

C. Atomic hydrogen adsorption at $1.0 < \Theta \leq 2.0$

From the previous discussions, it is concluded that the most stable adsorption site for H/Zr(0001) system is the on-surface hcp site and a large energy barrier has to be overcome to penetrate from the on-surface fcc site to the subsurface octahedral site in the coverage regime of $0 < \Theta \leq 1.0$. This means that at low temperature, the H adatoms will mostly reside on the Zr(0001) surface and a spontaneous penetration process can hardly occur at $0 < \Theta \leq 1.0$. Accordingly, it is necessary for us to carry out an extensive investigation on the atomic hydrogen adsorption in the wider coverage range of $1.0 < \Theta \leq 2.0$. One should notice that at present the exact experimental determination of saturation coverage is still unreasonable due to the limitation of the resolution and device factors. Thus, the theoretical study and prediction of surface hydrogenation are still meaningful at the present stage.

In this work, we take consideration into the four coverage configurations, i.e., $\Theta = 1.25$, 1.50, 1.75, and 2.00 in the use of a $p(2 \times 2)$ surface cell. At first, the initial positions of H atoms are set in the way that 1 ML H are placed at the surface hcp sites and the remaining (Θ-1) ML H are located at the surface fcc sites. This choice of the initial geometry is simply motivated by the low coverage result above that the on-surface hcp and fcc sites are more stable than the subsurface tetrahedral-II and octahedral sites. After the geometry relaxations for the four atomic structures, we calculate the adsorption energies, the first interlayer relaxations, and the H-Zr bond lengths all of which are listed in Table V. The atomic hydrogen positions after relaxation are still at the hcp and fcc site of the Zr(0001) surface. From Table V, one can see that the adsorption energy decreases at higher coverage showing that the stability of the atomic hydrogen adsorption on Zr(0001) surface is weakened as the coverage increases in the range of $1.0 < \Theta \leq 2.0$. Particularly, the topmost interlayer relaxation changes from contraction $\Delta_{12} = -5.333\%$ at $\Theta = 1.25$ to expansion $\Delta_{12} = +2.833\%$ at $\Theta = 2.00$. Needless to say, the larger interlayer expansion costs more energy, which will counteract the formation of the H/Zr(0001) adsorption structures in higher coverage, in good accordance with the adsorption energy results presented in Table V.

Furthermore, to study the possibility of the hydrogen penetration into the subsurface region at high coverage with the CINEB method, we continually consider two possible paths with 1 ML hcp and fcc H atoms separately covered on surface in the $p(2 \times 2)$ supercell. First for the structure with 1 ML on-surface hcp H atoms, the additional one hydrogen atom is placed initially at an on-surface fcc site and assumed to penetrate into the sub-surface octahedral site beneath. Then for the configuration with 1 ML on-surface fcc H atoms, the second proposed penetration path from the on-surface hcp site to the tetrahedral-I site beneath is considered as well. After the similar CINEB calculations, it is found that at this total coverage $\Theta = 1.25$, the incorporation barriers are only 0.18 eV and 0.14 eV correspondingly, in consistence with the previous calculated results.[15] So it is clearly seen that the hydrogen can diffuse into the sub-surface sites at higher coverage easily compared to the calculated results in the coverage regime of $0 < \Theta \leq 1.0$. As a result, we extend our discussion of the stability of co-adsorption configurations to higher coverages, namely, $1.0 < \Theta \leq 2.0$. We calculate the mixed structures with 1 ML hcp or fcc H atoms on the surface and a series of H coverage in the subsurface sites, given in Table VI. The results show that the most stable co-adsorption configuration is the mixed structure that the H atoms are placed at the hcp sites on surface and the octahedral sites in the subsurface. Meanwhile, for the same total coverage, the calculated adsorption energies of the most stable structures in Table VI are a little larger than the results from pure on-surface H adsorption given in Table V, indicating that the subsurface H can stabilize the adsorption structure. Therefore, it facilitates the H penetration and absorption in the subsurface and bulk region, showing that the Zr(0001) surface tends to accommodate the H atoms by forming the H-Zr-H trilayer as sandwich structure, which is good for improving the energetics for H uptake. The stabilization to form the sandwich structure H-Zr-H can be rationalized from the enhanced orbital hybridization between the adsorbate H atom and the substrate Zr atom, which is illustrated from the corresponding PDOS plotted in Fig. 7. The on-surface H hybridizes at higher energy levels between −5 eV and −4 eV, while the sub-surface H prevails in the range of −8 eV and −6 eV. With the increase of the sub-surface H

TABLE VI. The calculated adsorption energy E_{ad} (eV/atom) for the structures with 1 ML hcp or fcc H atoms on the surface and submonolayer subsurface octahedral, tetrahedral-I, and tetrahedral-II hydrogen, respectively. The corresponding total coverage is given at the bottom.

Sites	$\Theta_{sub} = 0.25$ (ML)		$\Theta_{sub} = 0.50$ (ML)		$\Theta_{sub} = 0.75$ (ML)		$\Theta_{sub} = 1.00$ (ML)	
	Hcp	Fcc	Hcp	Fcc	Hcp	Fcc	Hcp	Fcc
Octa	0.964	0.909	0.922	0.824	0.835	0.764	0.801	0.722
Tetra-I	0.892	0.952	0.782	0.906	0.708	0.871	0.666	0.855
Tetra-II	0.956	0.918	0.882	0.847	0.829	0.801	0.791	0.771
Θ_{total}	1.25		1.50		1.75		2.00	

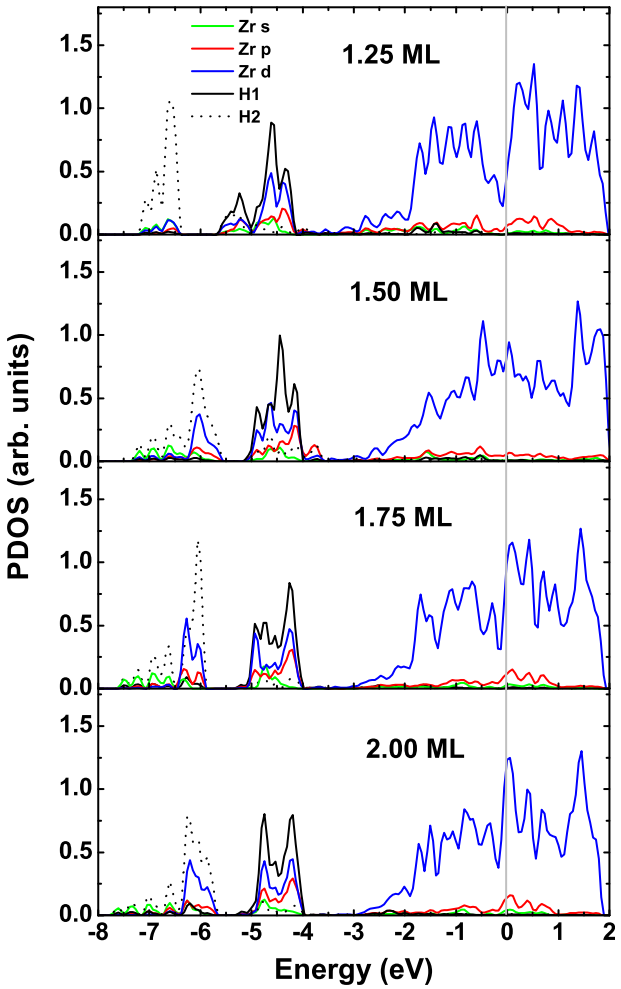

FIG. 7. The PDOS for the on-surface hydrogen at the hcp site (noted as H1), the subsurface hydrogen at the octahedral site (noted as H2), and the topmost Zr atom at the coverage of 1.25, 1.50, 1.75, and 2.00 ML, respectively. The Fermi energy is set at zero.

coverage, the Zr-*4d* and H-*1s* atomic orbital interaction becomes much more hybridized. However, the overall energetics of the H-Zr system are improved as the increased subsurface H atoms gradually induce the large distortion energy which is reflected from the adsorption energy variation with the coverage presented in Table VI. Based on this observation, we do not consider the coverage region of $\Theta > 2.0$. In fact, we have already studied the electronic properties of the face-centered tetragonal ZrH_2.[28] Compared with the PDOS of the H-Zr-H sandwich structure at the coverage $\Theta = 2.00$ ML, it is definitely instructive to help understand the hydrogenation of the Zr(0001) surface in depth, which is characterized by the occurrence of the surface hydride. It can be found that the main distribution feature of the PDOS for both the sandwich structure of H/Zr(0001) and the bulk ZrH_2 is very similar. For instance, the H-*1s* orbital and the Zr-*4d* hybridization appears as two prominent peaks, one at the energy range of -8 eV and -6 eV, the other one at the region of -6 eV and -4 eV. The Zr-*4d* occupation lies mainly at the high energy region. Consequently, it is reasonable to expect the formation of the surface hydride on the Zr(0001) surface with the similar chemical stoichiometry of the bulk ZrH_2. From this perspective, we can see that the surface hydride formation may act as the precursor for the transition to the bulk Zr hydride with the increase in hydrogen adsorption, which is greatly meaningful to make better understanding of the hydrogenation mechanism.

IV. CONCLUSION

In summary, we have systematically investigated the adsorption properties of atomic hydrogen on the Zr(0001) surface, as well as the energy barriers for atomic H diffusion and penetration through the first-principles DFT-GGA calculations. A wide range of the coverage from 0.11 to 2.00 ML is considered in detail by employing different surface cell models for the adsorption structures corresponding to the on-surface hcp and fcc sites, as well as the subsurface tetrahedral-I, tetrahedral-II, and octahedral sites. In the coverage regime of $0 < \Theta \leq 1.0$, the most stable equilibrium adsorption configuration among all possible pure adsorbed sites on surface and the co-adsorbed sites is the on-surface hcp site, followed by the fcc site on surface. Particularly, the atomic geometry, the work function, the charge density distribution, and the electronic structure upon the most stable adsorption have been studied carefully, which consistently show the fundamental influence both by the ionic and covalent bonding between the H adatom and surface Zr atoms. Furthermore, we have also calculated the MEPs of both surface diffusion and the surface-to-subsurface penetration. For the on-surface diffusion, it has been found that the hcp and fcc sites are the two local minima, while the bridge site is the saddle point along the diffusion path. The activation barriers for the surface diffusion from the hcp to fcc site are 0.29 eV at $\Theta = 0.25$ and 1.40 eV at $\Theta = 1.00$, respectively, implying that the surface diffusion tends to be much more difficult with increasing the hydrogen coverage in the $0 < \Theta \leq 1.0$ region. On the other hand, the activation barriers for the penetration from the on-surface fcc site to the subsurface octahedral site is largely increased with the hydrogen coverage. Additional calculations show that the penetration energy barriers are much lower if only one hydrogen penetrates into the subsurface at high hydrogen coverage. In the coverage range of $1.0 < \Theta \leq 2.0$, we also investigate the pure adsorbed on surface and the co-adsorption structures as well. Starting with the initial adsorption configurations that 1.0 ML H are placed on the surface hcp sites and (Θ-1) ML H are placed on the surface fcc sites, we find that after atomic relaxations, the stability of the H-Zr systems weakens as the coverage increases. Then the co-adsorption structure with 1.0 ML H residing on the surface hcp or fcc sites and the remaining of the (Θ-1) ML H occupying the sub-surface tetrahedral-I, tetrahedral-II, and octahedral sites are systematically calculated. It is shown that the most stable co-adsorption structure is the one with 1.0 ML H on surface hcp sites and the remaining (Θ-1) ML H located in the subsurface octahedral sites. The obtained adsorption energy results also indicate that the subsurface H can stabilize the adsorption structure as forming the H-Zr-H sandwich structure compared with the pure adsorption on the surface in the same coverage. Therefore, it facilitates the H penetration and absorption in the subsurface and bulk region. In addition, the resultant H-Zr-H

trilayer structure of the most stable co-adsorption configuration displays a similar PDOS spectra feature to the bulk ZrH_2. As a result, the present work would be highly helpful to understand the mechanism of the incipient hydrogenation of the Zr(0001) surface.

ACKNOWLEDGMENTS

This work was financially supported by NSFC under Grant Nos. 51071032 and 11275147. The computation work is partly supported by the cluster Hua-I in Xi'an Jiaotong University and the National Supercomputing Centre in Shenzhen. We are grateful for the fruitful discussions with Mr. J. M. Kebwaro.

[1]D. A. King and D. P. Woodruff, *The Chemical Physics of Solid Surfaces and Heterogeneous Catalysis* (Elsevier, Amsterdam, 1998).
[2]Y. Fukai, *The Metal Hydrogen System* (Springer-Verlag, 2005).
[3]P. Bouffioux and L. Legras, in *Proceedings of the International Topical Meeting on Light Water Reactor Fuel Performance* (Park City, Utah, 2000).
[4]R. L. Tapping, J. Nucl. Mater. **107**, 151 (1982).
[5]L.-M. Lin and R. E. Gilbert, Appl. Surf. Sci. **18**, 315 (1984).
[6]W. J. Peterson and R. E. Gilbert, Appl. Surf. Sci. **24**, 121 (1985).
[7]F. Vanini, St. Buchler, X.-N. Yu, M. Erbudak, L. Schlapbach, and A. Baiker, Surf. Sci. **189/190**, 1117 (1987).
[8]D. A. Asbury, G. B. Hoflund, W. J. Peterson, R. E. Gilbert, and R. A. Outlaw, Surf. Sci. **185**, 213 (1987).
[9]D. Khatamian and F. D. Manchester, J. Nucl. Mater. **166**, 300 (1989).
[10]C. S. Zhang, B. J. Flinn, K. Griffiths, and P. R. Norton, J. Vac. Sci. Technol. A **10**, 2560 (1992).
[11]A. Sawatzky and C. E. Cross, in *Twelfth International Symposium on Zirconium in the Nuclear Industry* (2000), Vol. 32, p. 1354.
[12]N. Stojilovic, E. T. Bender, and R. D. Ramsier, Prog. Surf. Sci. **78**, 101 (2005).
[13]C. Domain, R. Besson, and A. Legris, Acta Mater. **50**, 3513 (2002).
[14]L. Holliger, A. Legris, and R. Besson, Phys. Rev. B **80**, 094111 (2009).
[15]M. Yamamoto, S. Naito, M. Mabuchi, and T. Hashino, J. Phys. Chem. **96**, 3409 (1992).
[16]P. Zhang, S. X. Wang, C. H. He, and P. Zhang, J. Nucl. Mater. **418**, 159 (2011).
[17]G. Kresse and J. Furthmüller, Phys. Rev. B **54**, 11169 (1996).
[18]J. P. Perdew, K. Burke, and M. Ernzerhof, Phys. Rev. Lett. **77**, 3865 (1996).
[19]G. Kresse and D. Joubert, Phys. Rev. B **59**, 1758 (1999).
[20]J. Neugebauer and M. Scheffler, Phys. Rev. B **46**, 16067 (1992).
[21]H. J. Monkhorst and J. D. Pack, Phys. Rev. B **13**, 5188 (1976).
[22]M. Weinert and J. W. Davenport, Phys. Rev. B **45**, 13709 (1992).
[23]F. Birch, Phys. Rev. **71**, 809 (1947).
[24]Y. S. Zhao, J. Z. Zhang, C. Pantea, J. Qian, L. L. Daemen, P. A. Rigg, R. S. Hixson, G. T. Gray III, Y. P. Yang, L. P. Wang, and T. Y. Uchida, Phys. Rev. B **71**, 184119 (2005).
[25]M. Yamamoto, C. T. Chan, and K. M. Ho, Phys. Rev. B **50**, 7932 (1994).
[26]G. Jomard, T. Petit, L. Magaud, and A. Pasturel, Phys. Rev. B **60**, 15624 (1999).
[27]L. G. Hector, Jr., J. E. Herbst, W. Wolf, P. Saxe, and G. Kresse, Phys. Rev. B **76**, 014121 (2007).
[28]P. Zhang, B. T. Wang, C. H. He, and P. Zhang, Comput. Mater. Sci. **50**, 3297 (2011).
[29]G. Henkelman, B. P. Uberuaga, and H. Jonsson, J. Chem. Phys. **113**, 9901 (2000).